CONF-960502--6

SAND96-0802C

ION IMPLANTATION IN COMPOUND SEMICONDUCTORS FOR HIGH-PERFORMANCE ELECTRONIC DEVICES

J. C. Zolper, A. G. Baca, M. E. Sherwin,
and J. F Klem
Sandia National Laboratories
Albuquerque, NM 87185-0603

Advanced electronic devices based on compound semiconductors often make use of selective area ion implantation doping or isolation. The implantation processing becomes more complex as the device dimensions are reduced and more complex material systems are employed. We review several applications of ion implantation to high performance junction field effect transistors (JFETs) and heterostructure field effect transistors (HFETs) that are based on compound semiconductors, including: GaAs, AlGaAs, InGaP, and AlGaSb.

INTRODUCTION

Ion implantation has been widely used in electronic and photonic devices based on compound semiconductors. Generally, the implantation process serves one of three functions. First, selective area implant doping is used to form low resistance contact regions in Field Effect Transistors (FETs), Heterojunction Bipolar transistors (HBTs), or lasers [1-5]. Selective area doping is also used in FETs to form precisely controlled channel or lightly doped drain (LDD) regions [6]. Second, implantation is employed to form locally high resistance regions for inter-device isolation such as in integrated FET circuits or for current guiding in lasers [7-12]. Third, ion implantation can be used to promote local area inter-diffusion or mixing of the host atoms to alter the local bulk properties of the semiconductor [13].

In this paper we focus on specific examples of using ion implantation for controlled, selective area doping. We begin by examining the key features in achieving high performance ion implanted GaAs Junction Field Effect Transistors (JFETs) that rely on shallow, abrupt p-type doping profiles as well as abrupt channel doping. The utility of heavy ion implantation (Zn and Cd) along with the co-implantation of P will be presented. The benefits of C-implantation to realized optimum channel profiles will also be discussed.

In a second area of study, we address the issues associated with implant doping of advanced ternary compound semiconductors materials such as AlGaAs, AlGaSb, and InGaP that are potential barrier layers for heterostructure field effect transistors (HFETs). The ability to selectively dope these barrier layers will enable improved HFET designs.

IMPLANTATION DOPING FOR GaAs JFETs

Figure 1 shows a schematic representation of a self-aligned GaAs JFET where all doping is done by ion implantation [5]. This structure overcomes several of the traditional short-comings of non-self-aligned or diffused junction JFETs such as an increased gate-to-source capacitance (C_{GS}) due the p/n junction gate and gate length broadening during the p^+

gate formation. The attributes of this structure have been well documented elsewhere for devices with gate lengths down to ~ 0.7 μm [14,15]. To extend this structure to sub-half-micron gate lengths, both the vertical and lateral the doping profile must be modified. For the vertical profile, the p^+-gate region must be made very shallow while still maintaining high doping at the surface to insure an ohmic gate contact. The channel profile also becomes more critical at short gate lengths with abrupt doping being required to reduce short channel effects and achieve good carrier confinement. The lateral n-type doping profile must also be modified for short gate operation to minimize hot carrier effects on the drain side of the gate and impact ionization to reduce short channel effects and improve the breakdown voltage. In this paper we discuss experimental improvements to the vertical doping profile. Optimization of the lateral profile will be presented elsewhere [16].

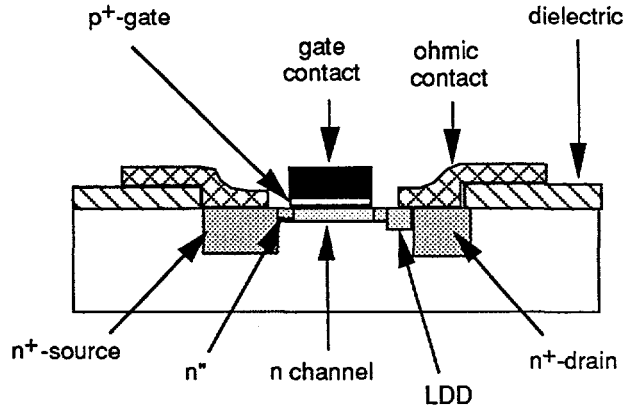

Fig 1: Schematic of self-aligned GaAs JFET with vertical and lateral doping modified for short gate operation.

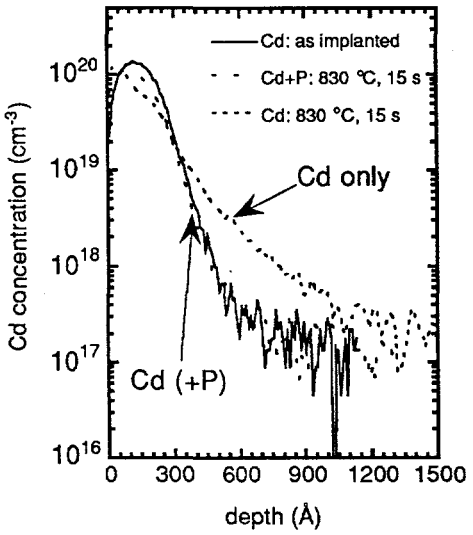

Fig 2: SIMS profiles of Cd-implanted GaAs (45 keV, $3x10^{14}$ cm^{-2}) as-implanted, Cd-only annealed at 830 °C, and co-implanted with P ($^{62}P_2$: 45 keV, $3x10^{14}$ cm^{-2}) annealed at 830 °C.

While initial work on the JFET structure in Fig. 1 employed Mg-implantation to form the p^+-gate region later generations demonstrated the utility of using the heavy acceptor species of Zn and Cd [14,15,17]. Figure 2 shows secondary ion mass spectroscopy (SIMS) profiles for the Cd-gate implant either alone or with a P co-implant. The use of P along with Cd is seen to markedly reduce the in-diffusion of Cd. The reduction in diffusion is critical to achieving the required abrupt p/n junction gate. Using a Cd-implanted Gate, a p/n junction depth of 35 nm has been demonstrated after the 830 °C activation anneal.

To achieve good electron confinement in the channel of a short gate JFET or MESFET, backside confinement is required. For all implanted device this is typically achieved by implanting a buried p-region below the channel. Traditionally this implant has been accomplished with Be or Mg[18]. However, as the FET gate length is reduced and better channel confinement is needed, an increase in the Be or Mg dose beyond

the point of achieving a completely depleted region will degrade the high-frequency performance. Therefore, for Be or Mg backside implants there is clear trade-off between optimizing the DC performance as measured by achieving a low output conductance (g_{DS}) and sub-threshold slope and optimizing the high-frequency performance as measured by the unity current cut-off frequency (f_t) and maximum oscillation frequency (f_{max}).

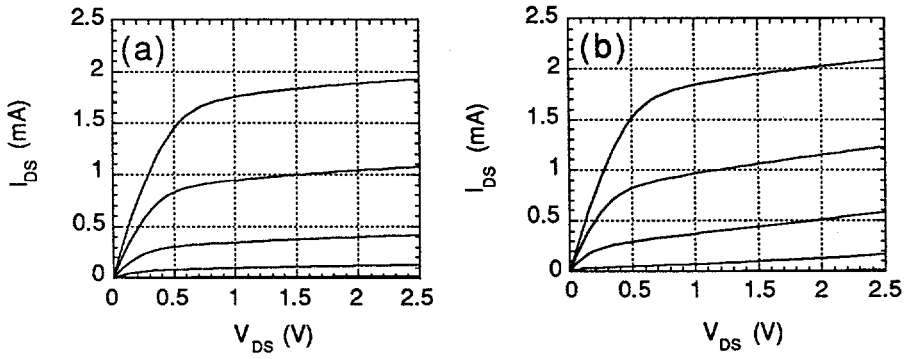

Fig 3: 0.7 μm x 50 μm all implanted GaAs JFETs with either a) Mg or b) C backside implants at a dose of $3x10^{12}$ cm^{-2}.

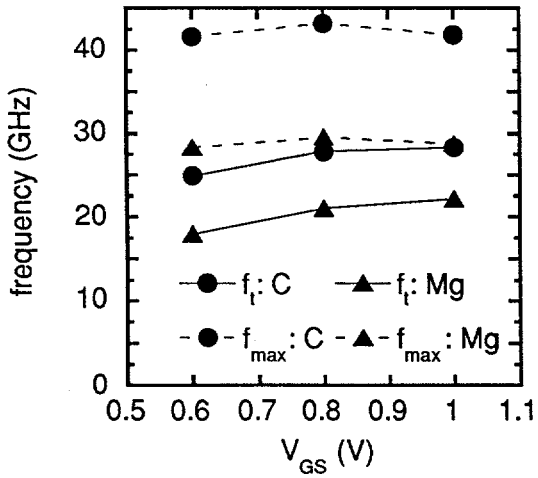

Fig 4: f_t and f_{mAx} versus gate bias for 0.7 μm GaAs JFETs with either Mg or C backside implants at a dose of $3x10^{12}$ cm^{-2}.

One way to relax this trade-off in DC and high-frequency performance is to use C-implantation to form the backside confinement region [19]. Since C must occupy an As-vacancy in GaAs to be an active acceptor and As-vacancies have a higher energy of formation than Ga-vacancies [20], C implanted by itself in GaAs displays an activation efficiency of typically less than 10% [21]. However, when a co-implant is performed along with C this activation efficiency can be markedly improved [22]. Furthermore, C will act as an effective compensator of implanted Si in the same way that a co-implant improves its activation efficiency [23]. Figure 3 shows the DC performance of 0.7 μm GaAs JFETs with either Mg or C-backside implants at a dose of $3x10^{12}$ cm^{-2}. Both devices in Fig. 3 have comparable DC performance when the slight differences in their threshold voltage are accounted for. In particular, they both have g_m and I_{DS} at 0.8 above V_{TH} of 200-210 mS/mm and 100 mA/mm, respectively. Further, the g_{DS} for both JFETs is 6-9 mS/mm and the sub-threshold slope is 80-90 mV/decade. Now in Fig. 4, the high-frequency performance metrics f_t and f_{max} are compared for the same devices. The JFET with the C-implant has a 28% high f_t and a 46% higher f_{max} than the Mg-implanted device. These improvements can be traced to lower values for the capacitances in the C-JFET that results from the lower activation of C, as compared to Mg,

below the n-type channel. This lower p-type doping below the channel in the C-implanted JFET reduces the junction capacitance for this backside junction. This effect will become more important for shorter gate length FETs where good DC performance will require higher dose backside implants. In fact, 0.3 μm GaAs JFETs have now been demostrated with excellent DC and high-frequecny (f_t = 49 Ghz) performance using a C-backside implant [16].

N-TYPE IMPLANT DOPING OF AlGaAs and InGaP

Both AlGaAs and InGaP used as barrier layers in n-channel HFETs and confinements layers in lasers. Selective area doping is desirable in both devices. First, we present results for a comprehensive study of Si-implantation doping of $Al_xGa_{1-x}As$ for $0 \leq x \leq 0.7$ [24]. By studying the activation properties for a range of Al-compositions we are able to separate donor activation and ionization effects. Second, results for Si-implantation in $In_{0.5}Ga_{0.5}P$ are given and the beneficial effects of P co-implantation are presented [25].

Si-implantation doping of $Al_xGa_{1-x}As$

Experimental Approach:

500 nm thick undoped AlGaAs layers were grown at 590 °C in a Varian Gen II MBE reactor on semi-insulating (100) GaAs substrates. A 200 nm undoped GaAs buffer was grown prior to the AlGaAs layer and a 5 nm GaAs cap layer was grown on top of the AlGaAs to inhibit oxidation. This MBE system has been used to grow high mobility AlGaAs/GaAs two dimensional electron gas structures with 77 K mobilities in excess of 10^6 cm^2/Vs demonstrating the high quality of the AlGaAs/GaAs material grown in this system [26]. ^{29}Si-implants were performed in a non-channeling direction at an energy of 100 keV at a dose of either $5.6x10^{12}$ or $2.8x10^{13}$ cm^{-2}. These doses are in the range used for FET channel and LDD formation or source/drain formation, respectively. Beam currents were kept below 0.1 $\mu A/cm^2$ to minimize sample heating and in-situ annealing. The estimated ion peak range is at 100 nm from the surface with a corresponding peak concentration of ~$1.8x10^{18}$ cm^{-3} for the higher dose samples. This concentration level is in the range where Si doping starts to saturate in GaAs [27]. Annealing was performed for 15 s in flowing Ar in a SiC coated graphite susceptor that had been precharged with As [28]. Room temperature and variable temperature (T = 77 to 400 K) Hall measurements were done using Van der Pauw Hall samples with In/Sn contacts alloyed at the corners of each sample at 400 °C for 1 min.

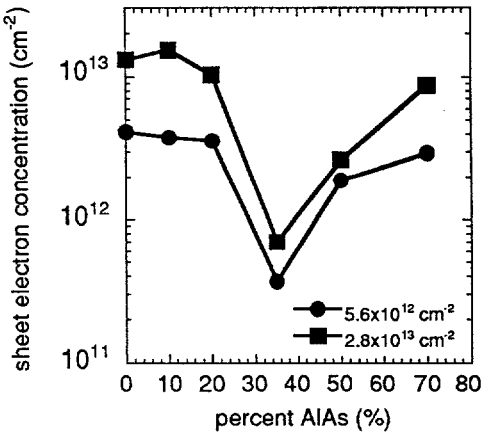

Fig 5: n_s versus % AlAs for Si-implanted AlGaAs at a dose of 5.6 or $28x10^{12}$ cm^{-2} at 100 keV and annealed at 900 °C.

Experimental Results And Discussion:

Figure 5 shows n_s versus %AlAs for the samples annealed at 900 °C. This temperature was determined to yield a maximum value of n_s for this implant dose. n_s is seen to be relatively constant dose out to 20% AlAs, dramatically decreases at 35% AlAs, and then increases at the higher Al-fractions (50 and

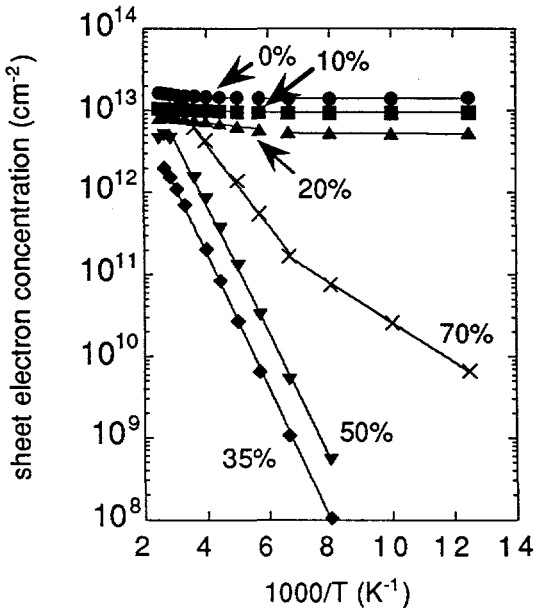

Fig 6: Arrhenius plot of n_s for the various high dose Si- AlGaAs samples annealed at 900 °C.

70% AlAs. The reason for these variations will be discussed in more detail shortly.

Figure 6 shows an Arrhenius plot of n_s for all the samples shown in Figure 5. The apparent donor ionization energy (E_d) can be estimated assuming:

$$n_s \propto \exp\left(\frac{-E_d}{kT}\right) \qquad (1)$$

The apparent ionization energy levels are listed in Table I, along with η_{eff}. Our values of E_d agree well for those reported for epitaxial Si-doped AlGaAs [29]. The 35 and 50% samples are seen to have similar ionization energy levels near 160 meV while the 70% sample has two levels at 86 and 55 meV. The two levels in the 70% sample correspond to the deep DX level (86 meV) and the hydrogenic donor level (55 meV) corresponding to different local Al and Ga environments about the Si atoms. For the 35 and 50% samples the free electrons all freeze-out into the deep DX level and the shallow donor level is not seen. Since the ionization energies are similar in the 35 and 50% samples, the ionization energy levels alone do not explain the effective activation efficiency dependence on Al-fraction shown in Fig 5. That is, based solely on the ionization energy, the 35 and 50% samples should both have similarly low activation but this is seen not to be the case from Table I.

Table I: Summary of ionization energies and effective activation efficiency of Si-implanted AlGaAs for the two doses studied.

%AlAs	apparent ionization energy, E_d (meV)	η_{eff}[a] $\phi = 5.6\times10^{12}$ cm^{-2}	η_{eff}[a] $\phi = 2.8\times10^{13}$ cm^{-2}
0	3.2	74.3	46.8
10	4.3	67.9	54.6
20	9.2	64.3	36.8
35	162	6.6	2.5
50	155	34.1	9.5
70	86, 55	52.8	31.1

[a] $\eta_{eff} = (n_s/\phi)\times100$

Figure 7 shows the dependence of the conduction band density-of-states in AlGaAs versus %AlAs based on the expression given below [30]:

$$N_c \equiv 2\left(\frac{2\pi m_{de} kT}{h^2}\right)^{3/2} M_c \quad (2)$$

where M_c is the number of equivalent minima in the conduction band and m_{de} is the density-of-states effective mass given by

$$m_{de} = (m_e^{\Gamma} m_e^{X} m_e^{L})^{1/3} \quad (3)$$

where m_e^{Γ}, m_e^{X}, and m_e^{L} are the effective electron mass in each of the energy bands and vary with Al-composition as follows [31]:

$$m_e^{\Gamma} = 0.067 + 0.83x \quad (4a)$$

$$m_e^{X} = 0.32 - 0.06x \quad (4b)$$

$$m_e^{L} = 0.11 + 0.03x \quad (4c)$$

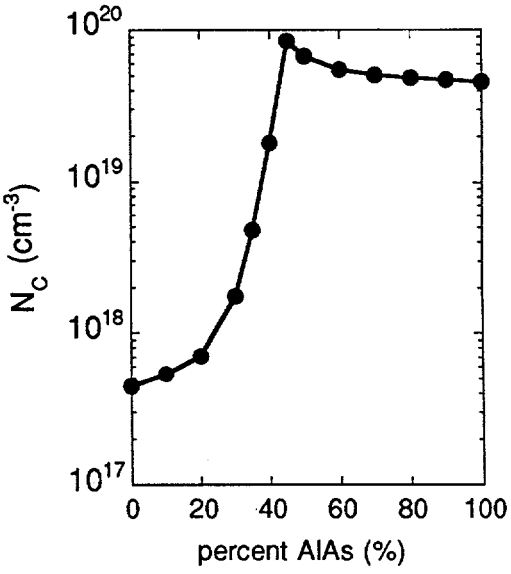

Fig 7: AlGaAs conduction band density-of-state versus % AlAs .

Other terms in Eqn 2 have their usual meaning. The free electron density (n) can then be expressed as:

$$n = N_c \exp\left(\frac{-(E_c - E_f)}{kT}\right) \quad (5)$$

where E_c is the conduction band minimum energy. The position of the Fermi level (E_f) can be solve for from the following expression for the density of ionized donors:

$$N_d^{+} = N_d\left[1 - \frac{1}{1 + \frac{1}{g}\exp\left(\frac{E_d - E_f}{kT}\right)}\right] \quad (6)$$

assuming the implanted layer thickness is equal to two standard deviations of the profile (t_{imp} = two implant straggles = $2\Delta R_p$) and N_d = (implanted dose)/t_{imp} . g is the electron ground state degeneracy and is equal to 2. E_d is the donor ionization energy listed in Table I. We further assume $N_d >> N_a$ and take the density of ionized donors to be equal to the measured sheet electron concentration divided by t_{imp}.

Figure 8 is a plot of calculated n from Eqn 5 and measured n ($n=n_s/t_{imp}$) versus %AlAs for the high dose samples at 300 K. The trend of electron concentration versus %AlAs, particularly the pronounced minimum at 35% AlAs, is consistent between the calculated values and measured data. However, the lack of absolute agreement between the theory and experiment is up to an order-of-magnitude and has several possible origins. First, as already stated, Eqn 5 is only an approximation that does not account for

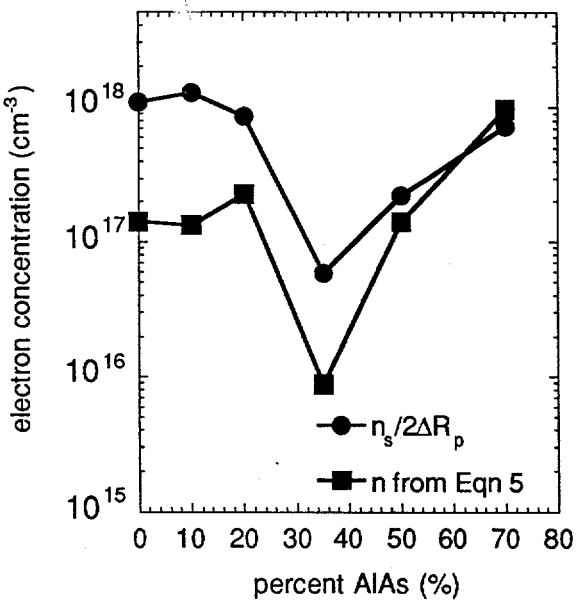

Fig 8: Calculated and measured n_s versus %AlAs for Si-implanted AlGaAs

compensation effects. Second, previous work on epitaxial AlGaAs has shown the difficulty in achieving absolute agreement between a theoretical density-of-states treatment of electron concentrations and the measured Hall concentration even when a full charge balance description is employed that includes acceptor compensation [32]. In that work a difference of an order-of-magnitude was reported between theory and Hall data. The lack of agreement is likely the result of the complex band structure of AlGaAs. Third, the 0, 10 and 20% samples will be degenerately doped since N_c is only ~$7x10^{17}$ cm^{-3} at 20% AlAs. Therefore, Eqn 6 does not yield the correct Fermi level position. Fourth, for implanted material several additional factors can be expected to affect the electron profile. For example, since the electron distribution is not uniform the mobility and compensation ratio is expected to vary throughout the profile. The Hall measurement also will only yield an average value for electron concentration and mobility that at best can be treated with a two band conduction model but in practice is not readily separated into its component parts. Finally, the defects generated during the implantation process which can act as either compensating acceptors or as scattering centers that degrade the electron mobility are most likely not the same in the different Al composition samples. Therefore, it is not clear that assuming a set compensation ratio over the entire compositional range is valid or useful.

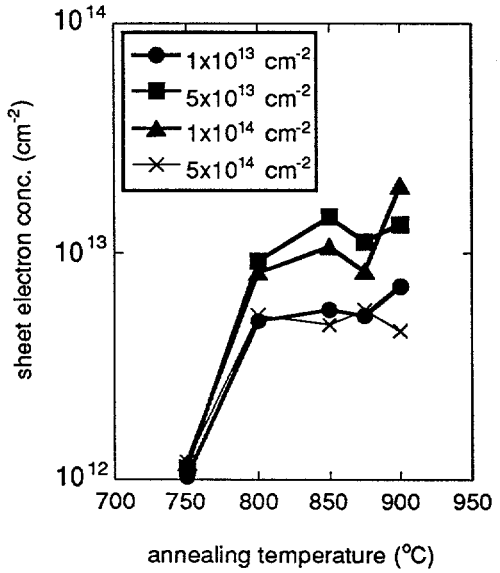

Fig 9: n_s versus annealing temperature for Si-implanted

Despite the shortcomings to the theory just discussed, the general variation in electron concentration evident in Fig. 5 can be qualitatively explained by the combined ionization energy and density-of-states treatment. We feel this treatment, although not absolute, is the most appropriate approach for explaining the Si-implantation results in AlGaAs.

Si/P Implants in $In_{0.5}Ga_{0.5}P$

Experimental:

InGaP at the doses listed.$In_{0.5}Ga_{0.5}P$ layers were grown at 640 °C by metalorganic

chemical vapor deposition (MOCVD) on (100) semi-insulating GaAs in an Emcore rotating disk reactor. The source gases were trimethylgallium, trimethlyindium, arsine, and phosphine. X-ray measurements confirmed that the films were lattice matched to the GaAs substrate within 0.22% for InGaP. ^{29}Si implants were performed in a nonchanneling direction at 90 keV at one of four doses (1, 5, 10, or $50x10^{13}$ cm^{-2}). P co-implants were done at 100 keV to overlay the Si-profile and at five multiples of the Si-dose (0, 0.5, 1.0, 1.5, or 2.0). After implantation, samples were annealing in a SiC coated graphite susceptor in flowing Ar for 15 s at the prescribed temperature ± 5°C. Prior to heating a three cycle pump/purge sequence is employed to reduce background oxygen levels. Room temperature and variable temperature Hall measurements were performed in a van der Pauw configuration with In/Sn or In/Pb contacts alloyed at the corners of the samples at 400 °C for 1 min. We estimate the accuracy of the Hall data to be ±10%.

Figure 9 shows the sheet electron concentration (n_s) versus annealing temperature for Si-implanted InGaP at four doses. n_s is seen to reach a maximum value of $1.33x10^{13}$ cm^{-2} in the range of 850 to 900 °C for a dose of $5x10^{13}$ cm^{-2} which is consistent with the earlier results of Si-implanted InGaP [33]. At higher doses self compensation starts to occur as Si demonstrates an amphoteric behavior. As will be demonstrated next, this saturation level can be increased by the application of P co-implantation.

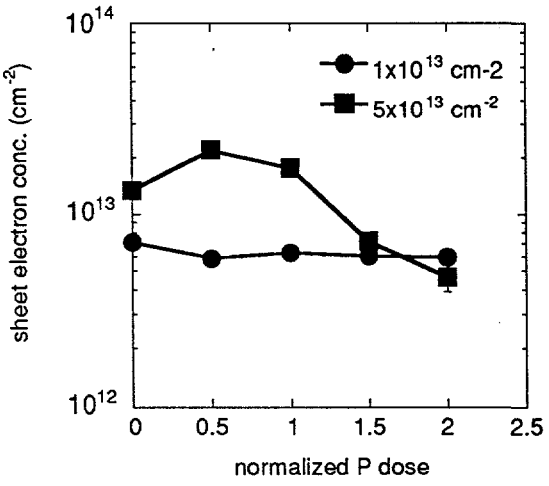

Fig 10: n_s versus normalized P-dose for Si-implanted InGaP at the two doses listed.

Figure 10 shows the change in n_s versus P co-implantation dose normalized to the Si-dose for two Si-doses in InGaP. These samples were all annealed at 900 °C for 15 s. Although n_s of the low dose InGaP samples does not change significantly with P co-implantation over the P-dose range studied; the InGaP material implanted with a dose of $5x10^{13}$ cm^{-2} demonstrates a dramatic increase in n_s for a P dose of $2.5x10^{13}$ cm^{-2} (0.5 times the Si-dose). The InGaP sample with 0.5xP has a 65% increase in n_s from the sample without P which corresponds to 44% activation in the co-implant sample. The decrease in n_s at higher P-doses can be explained by local deviation of stoichiometry due to excess P or to the additional implant damage not being completely removed at the higher doses. The increase in n_s at 0.5xP corresponds to a 41% reduction in the sheet resistance from 530 to 310 Ω/□. Such a reduction will have a dramatic effect on the performance of a FET that incorporates a InGaP barrier layer and Si-implantation doping in the source and drain regions. The improvements seen here for n_s in InGaP are slightly higher than that seen for Si/P implants in GaAs (~50%) [34] and InP (~30%) [35].

The effect of the P co-implantation can be explained via two possible mechanisms, both of which increase the probability of the Si-ion to occupy the column III sublattice and act as a donor [17]. The mechanisms both stem from the realization that as-implanted material will consist of both In, Ga, and P vacancies and interstitials due to the radiation

damaged introduced in the implantation process. In addition, since the host elements have significantly different atomic masses, local stiochiometry variations will exist in the crystal after implantation due to the different amount of recoil of each element. The first possible mechanism is that the P-ion will fill P-vacancies thereby reducing the P-vacancy concentration available for the Si-ions to occupy and act as acceptors instead of column III donors. Second, the P-ions may tie up interstitial In and Ga thereby rebuilding the lattice and reducing the competition between the host column III-elements and implanted Si atoms for occupation of the vacant In- and Ga-sites. The P-implantation will also help to restore the local crystal stiochiometry.

C-Implantation Doping of $Al_{0.75}Ga_{0.25}Sb$

P-channel field effect transistors (FETs) based on the nearly lattice matched GaSb/InAs/AlSb material system offer higher performance than other material systems due to the high hole mobility in GaSb [36]. GaSb has a low-field hole mobility of 850 cm^2/V-s, which is over twice that of GaAs and one of the highest of any III-V compound semiconductor. When coupled with an InAs n-channel FET, the GaSb p-channel FET has been the focus of a complimentary III-V semiconductor based circuit technology [37,38]. In the GaSb-channel FET, $Al_XGa_{1-X}Sb$ with a high Al-fraction is a candidate material for the barrier layer between the channel and gate electrode [39,40]. To reduce the source and drain resistances of the p-FET, it is desirable to be able to dope $Al_XGa_{1-X}Sb$ selectively by ion implantation.

We have studied p-type implantation doping of $Al_{0.75}Ga_{0.25}Sb$ with Be, C, Mg and Zn [41]. We review here the results for C-implantation doping in this material and show its acceptor nature. This is the first demonstration of C-doping of $Al_{0.75}Ga_{0.25}Sb$.

Experimental:

2 μm thick undoped $Al_{0.75}Ga_{0.25}Sb$ layers were grown in a Varian Gen-II molecular beam epitaxial reactor on (100) GaAs substrates with a "low-temperature" effusion cell producing a Sb_4 flux [39]. A buffer structure consisting of a 100 nm GaAs layer, a 50 nm GaSb "smoothing" layer, a 9 period AlSb(6 nm)/GaSb(6 nm) superlattice buffer, and a 30 nm AlSb layer was incorporated to reduce the lattice mismatch induced dislocation density.

^{12}C-implants were performed at a dose of 1 or 10 $x10^{13}$ cm^{-2} at an energy of 70 keV to place the peak at approximately 150 nm. The activation anneals were performed in a SiC coated graphite crucible that had been precharged with Sb by loading excess GaSb in the crucible and annealing at 700 °C for 1 min prior to annealing the implanted samples. The electrical characterization was performed by room temperature Hall measurements on samples in a van der Pauw configuration with In contacts on the corners of approximately 5 mm x 5 mm samples annealed at 240 °C for 1 min. SIMS measurements were done on as-implanted and annealed samples to characterized the redistribution properties of C.

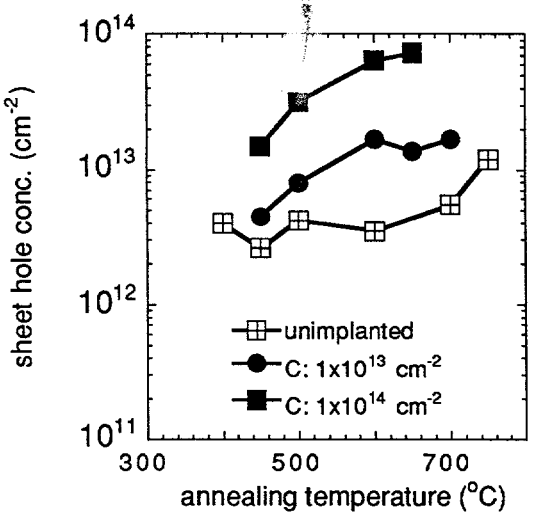

Fig 11: p_s versus annealing temperature for C-implanted AlGaSb at the doses listed.

Results and Discussion:

Figure 11 displays the sheet hole concentration (p_s) versus annealing temperature for $Al_{0.75}Ga_{0.25}Sb$ either unimplanted or implanted with one of two C doses ($1x10^{13}$ or $1x10^{14}$ cm^{-2}) at 70 keV. At 500 °C the lower dose C-implanted sample has $p_s = 8x10^{12}$ cm^{-2} that corresponds to an effective activation of 40 % when p_s of the unimplanted sample ($4x10^{12}$ cm^{-2}) is subtracted out. At 600 °C the lower dose C-sample achieves $p_s = 1.7x10^{13}$ cm^{-2} that, even when accounting for the p-type nature of the unimplanted sample, corresponds to an apparent 130% activation efficiency.

This result suggests an anti-site defects (Ga_{Sb} or Al_{Sb}) may contribute to the hole conduction in excess of the implanted acceptor dose. The intrinsic hole conduction in GaSb has been attributed to Ga_{Sb} anti-site defects [42]. Similar defects (Ga_{Sb} or Al_{Sb}) may exist in $Al_{0.75}Ga_{0.25}Sb$ with their concentration enhanced as a result of implantation damage. It should be noted that the unimplanted material has a background $p_s \sim 4x10^{12}$ cm^{-2} that can be expected to exist in the implanted material as well and contribute to the p-type conduction.

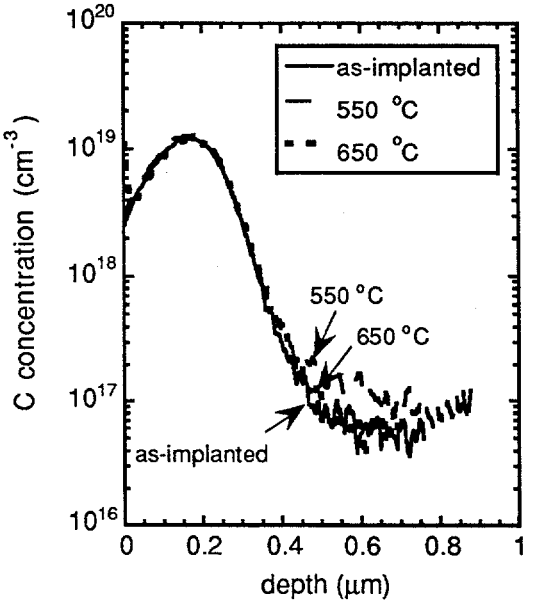

Fig 12: SIMS profiles for C-implanted AlGaSb ($1x10^{14}$ cm^{-2}, 70 keV) as-implanted or annealed at 550 or 650 °C.

For the higher dose C-implant a 25% apparent activation is seen at 500 °C and 60% apparent activation is seen at 600 °C. This activation starts to saturate at 650 °C near 70%. For some applications a 500 °C anneal may yield sufficient p-type conduction for a InGaSb-based, p-FET thus avoiding any potential degradation of the transport properties of the channel at higher temperatures [41].

The SIMS profiles for C-implanted (70 keV, $2.5x10^{14}$ cm^{-2}) $Al_{0.75}Ga_{0.25}Sb$ are shown in Fig. 12. The profiles for the annealed samples (550 and 650 °C) are almost indistinguishable from the as-implanted profile. The lack of C-diffusion even for a the high dose sample is consistent with the low diffusion coefficient for C in other III-V semiconductors [43]. This lack of diffusion along with close to 70% activation at 600 °C for a dose of $1x10^{14}$ cm^{-2} makes C very attractive for p-type implantation doping of AlGaSb.

CONCLUSION

Ion implantation doping has been shown to be applicable to an array of compound semiconductor materials. In particular, Zn and Cd implantation along with a P co-implantation in GaAs was shown to effective for producing the shallow p^+-gate region of JFETs. The utility of C-implantation was seen both for use in forming the backside channel confinement region for a JFET and for p-type doping of $Al_{0.75}Ga_{0.25}Sb$. Comprehensive results for Si-implantation doping of AlGaAs were also presented and explained in terms of an ionization energy and density-of-states treatment. The activation efficiency of high dose S-implants in InGaP were shown to be enhanced by ~60% through an optimized dose P co-implantation. As has been the case in mature semiconductor technologies such as Si and GaAs, ion implantation processing can be expected to continue to play a critical enabling role for advanced device fabrication.

ACKNOWLEDGMENTS:

The authors gratefully acknowledge the technical assistance of J. Escobedo for ion implantation and G. Lopez for JFET processing. This work was supported by the Department of Energy under DOE contract #DE-ACO4-94AL85000

REFERENCES

[1] K. Daoud-Ketata, C. Dubon-Chevallier, and C. Besombes, IEEETrans. Elc. Dev. **8**, 205 (1987).

[2] S. J. Pearton, F. Ren, P. W. Wisk, T. R. Fullowan, R. F. Kopf, J.-M. Kuo, W. S. Hobson, and C. R. Abernathy, J. Appl. Phys. **62**, 698 (1991).

[3] J. P. de Souza and D. K. Sadana, IEEE Trans. Elec. Dev. **39**, 166 (1992).

[4] M. Feng and J. Laskar, IEEE Trans. Elec. Dev. **40**, 9 (1993).

[5] J. C. Zolper, A. G. Baca, R. J. Shul, A. J. Howard, D. J. Rieger, M. E. Sherwin, M. L. Lovejoy, H. P. Hjalmarson, B. L. Draper, J. F. Klem, and V. M. Hietala, IEEE Trans. Elec. Dev, **41**, 1078 (1994).

[6] A. I. Akinwanda, K. L. Tan, C. H. Chen, and P. J. Vold, IEEE Elec. Dev. Lett. **9**, 275 (1988).

[7] D. C. D'Avanzo, IEEE Trans. Elec. Dev. **29**, 1051 (1982).

[8] F. Ren, S. JH. pearton, W. S. Hobson, T. R. fullowan, J. Lothian, and A. W. Yanof, Appl. Phys. Lett. **56**, 860 (1990).

[9] J. C. Zolper, A. G. Baca, and S. A. Chalmers, Appl. Phys. Lett. **62**, 2536 (1993).

[10] S. J. Pearton, Mat. Sci. Rep. **4**, 313 (1990).

[11] M. Orenstein, N. G. Stoffel, A. C. Von Lehmen, J. P. Harbiunson, and L. T. Florez, Appl. Phys. Lett. **59**, 31 (1991).

[12] K. L. Lear, R. P. Schneider, K. D. Choquette, S. P. Kilcoyne, J. J. Figiel, and J. C. Zolper, IEEE Photonic Tech. Lett. **6**, 1053 (1994).

[13] D. G. Deppe and N. Holonyak, Jr. J. Appl. Phys. **64**, R93 (1988).

[14] M. E. Sherwin, J. C. Zolper, A. G. Baca, R. J. Shul, A. J. Howard, D. J. Rieger, J. F. Klem, and V. M. Hietala, IEEE Elec. Dev. Lett. **15**, 242 (1994).

[15] J. C. Zolper, A. G. Baca, M. E. Sherwin, and R. J. Shul, Elec. Lett. **31**, 923 (1995).

[16] J. C. Zolper, A. G. Baca, V. M. Hietala, R. J. Shul, and M. E. Sherwin, submitted to Device Research Conf. 6/96.

[17] M. E. Sherwin, J. C. Zolper, A. G. Baca, T. J. Drummond, R. J. Shul, A. J. Howard, D. J. Rieger, R. P. Schnieder, and J. F. Klem, J. Elec. Mater. **23**, 809 (1994).

[18] K. Onodera, M. Tokumitsu, M. Tyomizawa, and K. Asai, IEEE. Trans. Elec. Dev. **38**, 429 (1991).
[19] J. C. Zolper, M. E. Sherwin, A. G. Baca, R. J. Shul, J. F. Klem, and V. M. Hietala, IEEE Elec. Dev. Lett. **15**, 493 (1994).
[20] R. W. Jansen and O. F. Sankey, Phys. Rev. B **39**, 3192 (1989).
[21] S. J. Pearton and C. R. Abernathy, Appl. Phys. Lett. **55**, 678 (1989).
[22] A. J. Moll, K. M. Yu, W. Walukiewicz, W. L. hansen, and E. E. Haller, Appl. Phys. Lett. **60**, 2383 (1992).
[23] R. M. Gwilliam, R. J. Wilson, T. D. Hunt, and B. J. Sealy, Nucl. Inst. and methods in Phys. Res., **B74**, 94 (1993).
[24] J. C. Zolper, J. F. Klem, A. G. Baca, M. E. Sherwin, M. J. Hafich, and T. J. Drummond, submitted to J. Appl. Phys. 2/96.
[25] J. C. Zolper and H. C. Chui, submitted to Appl. Phys. Lett. 3/96.
[26] J. F. Klem, private communication
[27] S. J. Pearton, J. Mod. Phys. B **7**, 4687 (1993).
[28] S. J. Pearton, A. Katz, and M. Geva, J. Appl. Phys. **68**, 2482 (1990).
[29] N. Chand, T. Henderson, J. Klem, W. T. Masselink, R. Fisher, Y. C. Chang, and H. Morkoç, Phys. Rev. B **30**, 4481 (1984).
[30] S. M. Sze, Physics of Semiconductor Devices, 2nd edition, (John Wiley, New York, NY, 1981) pp. 17- 24.
[31] S. Adachi, J. Appl. Phys. **58**, R1 (1985).
[32] S. P. Svensson and A. W. Swanson, J. Appl. Phys. **59**, 2870 (1986).
[33] S. J. Pearton, W. S. Hobson, J. M. Kuo, H. S. Luftman, A. Katz, and F. Ren, Appl. Phys. Lett. **60**, 1117 (1992).
[34] F. Hyuga, H. Yamazaki, K. Wanatabe, and J. Osaka, Appl. Phys. Lett. **50**, 1592 (1987).
[35] A. Dodabalapur and B. G. Streetman, J. Elec. Mat. **18**, 65 (1989).
[36] L. F. Luo, K. F. Longenbach, and W. I. Wang, IEEE Elec. Dev. Lett. **11**, 567 (1990).
[37] K. F. Longenbach, R. Beresford, and W. I. Wang, IEEE Trans. Elec. Dev. **37**, 2265 (1990).
[39] K. Yoh, H. Taniguchi, K. Kiyomi, and M. Inoue, Jap. J. Appl. Phys. **30** 3833 (1991).
[39] J. F. Klem, J. A. Lott, J. E. Schirber, S. R. Kurtz, and S. Y. Lin, J. Elec. Mat. **22** 315 (1993).
[40] L. F. Luo, R. Beresford, and W. I. Wang, Appl. Phys. Lett. **55**, 789 (1989).
[41] J. C. Zolper, J. F. Klem, A. J. Howard, and M. Hafich, J. Appl. Phys. **79**, 1365 (1996).
[42] D. Effer and P. J. Etter, J. Phys. Chem Solids, **25**, 451 (1961).
[43] C. R. Abernathy, S. J. Pearton, R. Caruso, F. Ren, and J. Kovalchik, Appl. Phys. Lett. **55**, 1750 (1989).